

# Directional analysis of 3D tubular structures via isotropic well-localized atoms

David Jiménez<sup>a</sup>, Demetrio Labate<sup>b</sup>, Manos Papadakis

<sup>a</sup>*Department of Mathematics, University of Costa Rica, Costa Rica*

<sup>b</sup>*Department of Mathematics, University of Houston, Houston, TX, 772014-3308, USA*

---

## Abstract

Accurate segmentation of 3D vessel-like structures is a major challenge in medical imaging. In this paper, we introduce a novel approach for the detection of 3D tubular structures that is particularly suited to capture the geometry of vessel-like networks, such as dendritic trees and vascular systems. Even though our approach relies on a system of isotropic multiscale analyzing atoms, we prove that their interaction via convolution with a tubular structure is equivalent to a set of directional atoms at various scales, automatically oriented along any possible direction and with cylindrical symmetry. This result sets the theoretical groundwork for the design of efficient discrete algorithms aiming at extracting the geometry of vessel-like structures in 3D medical images.

*Keywords:* Directional representations, isotropic filters, tubular structures, Laplacian filters, steerable filters

*2012 MSC:* 42C40

---

## 1. Introduction

This paper presents a new method for the detection and geometric characterization of tubular structures in 3D images. This study is motivated by the problem of segmenting and reconstructing the morphological properties of vessel-like structures in medical images, such as vascular networks in the lungs or the liver, dendritic arbors and axons in brain tissues and neuronal cultures.

---

*Email addresses:* david.jimenezlopez@ucr.ac.cr (David Jiménez ),  
dlabate@math.uh.edu (Demetrio Labate), mpapadak@math.uh.edu (Manos Papadakis)

Processing these types of images presents several challenges, due to the complex 3D topology and the significant variations in size, orientation and intensity contrast of the vessel-like structures that need to be detected in images. Due to large variations in size of objects of interest, a number of ideas based on multiscale analysis have been proposed for the analysis and the preprocessing of such data. Koller et al. [16], in particular, introduced a multiscale filter based on the eigenvectors of the Hessian matrix of the image, to detect highly elongated objects. Following this work, other successful studies have focused on the eigenvalues of the Hessian matrix to detect tubular structures (cf. [17] and references therein).

During the last decade, the emergence of more sophisticated multiscale methods has further expanded the range of tools available for the analysis of geometric features of multidimensional data. Among these methods there are several ‘directional’ representations where the analyzing functions are defined not only across several scales but also at several orientations, such as beamlets [6], ridgelets [3], curvelets [4] and shearlets [8, 21]. Thanks to a combination of multiscale analysis and directional sensitivity, these methods can provide highly sparse representations of images with edges [4, 8, 19]. Indeed, directional multiscale transforms derived from these representations can be especially effective at capturing the geometry of multidimensional singularities through their asymptotic decay at fine scales [5, 18]. These properties can be very useful in the analysis of biomedical images containing highly elongated structures as illustrated by recent applications to fluorescent images of brain tissue and neuronal cultures [20, 23, 24].

Remarkably, in this paper we show that it is possible to capture the geometric characteristics of a 3D tubular structure, regardless of its spatial orientation, using rather conventional multiscale 3D isotropic Laplacian filters. As we prove in this paper, when applied to tubular structures these filters act as two-dimensional Laplacians at the direction of the gradient of the intensity level of the image. In other words, the interaction via convolution of a set of isotropic multiscale atoms with a tubular structure is equivalent to the action of a set of directional multiscale 3D atoms, aligning themselves to the tubular structure and with cylindrical symmetry. Hence, the convolution of these atoms produce rotationally covariant outputs obeying very simple covariance rules (cf. Theorem 1 in Sec. 2), although the analyzing atoms of the underlying representation are not intrinsically steerable, in the sense that there is no external mechanism to steer them. They act as self-steerable atoms when they interact with tubular structures.

This finding is quite reminiscent of Marr’s claim that low-level vision is based on the detection of intensity changes of luminosity modeled by filtering an image with an isotropic Laplacian operator windowed by a two-dimensional isotropic Gaussian [22, p. 54]. Such models are supported by neurophysiological findings according to which the retinal photoreceptors are spatially organized ([7], Ch. 1, also see [22], pp. 64–65, and [25]) so that:

- (a) “They provide high or low spatial and temporal resolution images of every scene depending on the prevailing conditions of observation; the temporal resolution equips the eyes with the perception of motion and the capability of detecting sudden stimulus onsets, while the spatial resolution primarily contributes to object recognition ([7], Ch. 1);
- (b) edges (boundaries where the luminosity abruptly changes) are observed *regardless* of their orientation or topology.”

By no means we claim that our collection of isotropic atoms yields a directional representation in the sense of a ‘true’ directional multiscale systems, where the analyzing atoms range over a set of prescribed orientations. In fact, the directional sensitivity of our isotropic atoms only arises in the presence of tubular structures and we consider these atoms as *analyzing* elements only (they cannot be used for synthesis). Another difference is that ‘true’ directional multiscale transforms are able to detect location and orientation of edge singularities through their asymptotic decay at fine scales, while our approach does not detect edges (see also the related discussion in the last section) neither can it identify the local orientation of the tubular structure, but it is effective at capturing the geometry of tubular structures at a specific range of scales.

With respect to directional multiscale representations, isotropic multiscale filters have lower redundancy, leading to discrete implementations with lower computational cost. This can be a significant advantage especially for the processing of 3D data.

## 2. Directional filtering of tubular structures using isotropic atoms

We begin by introducing a generic class of tubular structures in  $\mathbb{R}^3$  that can be used to model dendritic branches of neurons, blood vessels and similar biological structures.

### 2.1. Modeling tubular structures

To define such tubular structures, we start by considering the *tubular segments* defined as tensor products of the form:

$$f_{l,L,r}(x, y, z) = g_{l,L}(x)g_r(y, z), \quad x, y, z, \in \mathbb{R}, r > 0, \quad (1)$$

where  $g_{l,L}$  is even, non-increasing on the positive half axis and satisfies

$$\begin{aligned} g_{l,L}(x) &= 1 & \text{if } 0 \leq x \leq l \\ g_{l,L}(x) &> 0 & \text{if } l < x < L \\ g_{l,L}(x) &= 0 & \text{if } L \leq x; \end{aligned}$$

the second factor satisfies  $g_r(y, z) \geq 0$  and  $g_r(y, z) = 0$  when  $y^2 + z^2 \geq r^2$ .

In (1), the term  $g_{l,L}$  controls the length of the structure, which extends along the  $x$ -axis, while the second factor controls the decay of the image intensity values in a cross-section. In the following, we will assume that the first and second-order derivatives of  $g_{l,L}$  and of  $g_r$  are both absolutely integrable, so  $g_{l,L}$  and  $g'_{l,L}$  and  $g'_r$  are both absolutely continuous. In order to allow more flexibility in the shape of “tubular” cross sections, we make no special symmetry assumptions on the term  $g_r$ .

Clearly, the tubular segments given by (1) can be translated via the action of translation operators  $T_{\mathbf{x}_k}$ ,  $\mathbf{x}_k \in \mathbb{R}^3$ , defined by  $T_{\mathbf{x}_k}f(\mathbf{x}) = f(\mathbf{x} - \mathbf{x}_k)$  and re-oriented by means of rotations  $R_k \in SO(3)$ . For any such a 3D rotation matrix  $R_k$ , we define the rotation operator  $\mathcal{R}_k$  by  $\mathcal{R}_k f(x, y, z) = f(R_k(x, y, z))$ . Therefore, we define a *tubular structure*  $\mathcal{I}$  as finite sum of the form

$$\mathcal{I} = \sum_{k=1}^K a_k T_{\mathbf{x}_k} \mathcal{R}_k f_{l_k, L_k, r_k}, \quad (2)$$

where the terms  $f_{l_k, L_k, r_k}$  are tubular segments and the quantities  $a_k$  are strictly positive constants controlling the image intensity in each tubular segment.

This model of tubular structures is adequate, in particular, to model dendritic branches in neurons where the centerline can be approximated by a polygonal curve. In our model, the intensity value along the centerline of any component  $T_{\mathbf{x}_k} \mathcal{R}_k f_{l_k, L_k, r_k}$  is constant. Even though in typical fluorescent images of neurons the fluorescent signal intensity is not constant, it is reasonable to assume that the intensity value does not vary too rapidly so that we can assume it to be constant along the centerline of a tubular segment, if this is sufficiently short.

## 2.2. Analysis of tubular segments

We start by examining the action of a simple family of isotropic transformations on the tubular segments  $T_{\mathbf{x}_k} \mathcal{R}_k f_{l_k, L_k, r_k}$ , for generic  $\mathbf{x}_k \in \mathbb{R}^3$ ,  $R_k \in SO(3)$ .

Let  $\phi \in L^2(\mathbb{R}^3)$  be a radial function such that all its derivatives up second order are absolutely integrable and such that  $\xi \mapsto \|\xi\|^2 \hat{\phi}(\xi)$  is also absolutely integrable and bounded. Let  $h$  be defined by

$$\hat{h}(\xi) := \|\xi\|^2 \hat{\phi}(\xi), \quad \xi \in \mathbb{R}^3. \quad (3)$$

Using a change of variables and the radially of  $h$ , we observe that

$$\begin{aligned} (T_{\mathbf{x}_k} \mathcal{R}_k f_{l_k, L_k, r_k} * h)(\mathbf{x}) &= \int_{\mathbb{R}^3} f_{l_k, L_k, r_k}(R_k(\mathbf{x} - \mathbf{x}_k) - s) h(R_k^T s) ds \\ &= f_{l_k, L_k, r_k} * h(R_k(\mathbf{x} - \mathbf{x}_k)). \end{aligned} \quad (4)$$

Clearly, the same equality is also valid with  $\phi$  instead of  $h$ :

$$(T_{\mathbf{x}_k} \mathcal{R}_k f_{l_k, L_k, r_k} * \phi)(\mathbf{x}) = f_{l_k, L_k, r_k} * \phi(R_k(\mathbf{x} - \mathbf{x}_k)). \quad (5)$$

The continuity of  $f_{l_k, L_k, r_k}$  and the integrability of  $\hat{h}$  imply that

$$\begin{aligned} f_{l_k, L_k, r_k} * h(R_k(\mathbf{x} - \mathbf{x}_k)) &= \int_{\mathbb{R}^3} \hat{f}_{l_k, L_k, r_k}(\xi) \hat{\phi}(\xi) \|\xi\|^2 e^{2\pi i \xi \cdot (R_k(\mathbf{x} - \mathbf{x}_k))} d\xi \\ &= \Delta(f_{l_k, L_k, r_k} * \phi)(R_k(\mathbf{x} - \mathbf{x}_k)). \end{aligned}$$

Therefore, we conclude that

$$\begin{aligned} &(T_{\mathbf{x}_k} \mathcal{R}_k f_{l_k, L_k, r_k} * h)(\mathbf{x}) \\ &= \Delta(f_{l_k, L_k, r_k} * \phi)(R_k(\mathbf{x} - \mathbf{x}_k)) \\ &= \frac{\partial^2}{\partial x^2} (f_{l_k, L_k, r_k} * \phi)(\mathbf{x}_0) + \left( \frac{\partial^2}{\partial y^2} + \frac{\partial^2}{\partial z^2} \right) (f_{l_k, L_k, r_k} * \phi)(\mathbf{x}_0), \end{aligned} \quad (6)$$

where  $\mathbf{x}_0 = R_k(\mathbf{x} - \mathbf{x}_k)$ . Equation (6) shows that the 3D Laplacian of the filtered output of the tubular segment has two components: the axial and the cross-sectional 2D Laplacian. In Theorem 1 we prove that, if  $\mathbf{x}$  is sufficiently far from the endpoints of the tubular segment, the first term in (6) is negligible whereas the second term is practically equal to the 3D Laplacian. *This shows that the action of the isotropic filters on the tubular*

structure is essentially equivalent to the action of cylindrically symmetric directional filters. We also remark that, in the derivation of (6), we did not assume any symmetry in the cross-sections of the tubular structure  $f_{l,L,r}$ . We use the term ‘tubular’ for such structures without necessarily implying any type of symmetry (e.g., radial symmetry) in the cross section.

Before stating our main theorem, we need some preparation.

We pick an accuracy threshold  $\epsilon > 0$  and we assume that  $\mathbf{x}_0$  is sufficiently away from both ends of the support of the tubular segment  $f_{l_k,L_k,r_k}$ . This implies that the support of  $\phi$  is relatively smaller than the support of the tubular segment, so that  $|\mathbf{x}_0 \cdot \mathbf{e}_1| + r_0 < l$ . Therefore, with no loss of generality we can shift the axial center of the tubular segment from the origin to another point on the  $x$ -axis so that  $\mathbf{x}_0 = (0, y_{0,1}, z_{0,1})$ . Now, the integrability of  $\xi \mapsto \|\xi\|^2 \hat{\phi}(\xi)$  and the Riemann-Lebesgue lemma imply that there exists  $r_0 > 0$  such that  $|D^\alpha \phi(\mathbf{y})| < \min\{\epsilon/2L, \epsilon\}$ , if  $\|\mathbf{y}\| \geq r_0$  and  $|\alpha| \leq 2$ .

On the other hand, the integrability of the partial derivatives of  $\phi$  up to second order allows us to select  $r_0$  so that  $\int_{|x|>r_0} |D^\alpha \phi| < \epsilon$  for all  $|\alpha| \leq 2$ . These two observations are summarized in the following lemma.

**Lemma 1.** *Let  $\epsilon > 0$  and  $\phi \in L^1(\mathbb{R}^3)$  be a radial function such that  $\xi \mapsto \|\xi\|^2 \hat{\phi}(\xi)$  is absolutely integrable and  $D^\alpha \phi \in L^1(\mathbb{R}^3)$  for all  $|\alpha| \leq 2$ . Then there exists  $r_0 > 0$  such that:*

1.  $|D^\alpha \phi(\mathbf{y})| < \min\{\epsilon/2L, \epsilon\}$  if  $\|\mathbf{y}\| \geq r_0$  and  $|\alpha| \leq 2$ ;
2.  $\int_{|x|>r_0} |D^\alpha \phi| < \epsilon$ .

In other words, we can choose a filter  $\phi$  with sufficient smoothness and spatial localization. In practical situations, like the numerical examples which will be considered further below, we don’t use a single filter  $\phi$  but a set of filters ranging over different scales, from fine to coarse, provided that we maintain the requirement  $|\mathbf{x}_0 \cdot \mathbf{e}_1| + r_0 < l$ . Filters with bigger  $r_0$  are suitable for thicker and longer tubular segments while filters with smaller  $r_0$  are fit for short and thin tubular segments. This heuristic statement will be formalized in Proposition 1.

We are now ready to state the main result of this work establishing that the isotropic filters  $\phi$  and  $h$  act as directional filters when they are applied to a tubular segment.

In the following, we use the convention  $\mathbf{e}_1 = (1, 0, 0)$ ,  $\mathbf{e}_2 = (0, 1, 0)$  and  $\mathbf{e}_3 = (0, 0, 1)$  and we denote by  $x(\mathbf{x}_0)$ ,  $y(\mathbf{x}_0)$  and  $z(\mathbf{x}_0)$  the various coordinates of the vector  $\mathbf{x}_0 = R(\mathbf{x} - \mathbf{x}_k)$ .

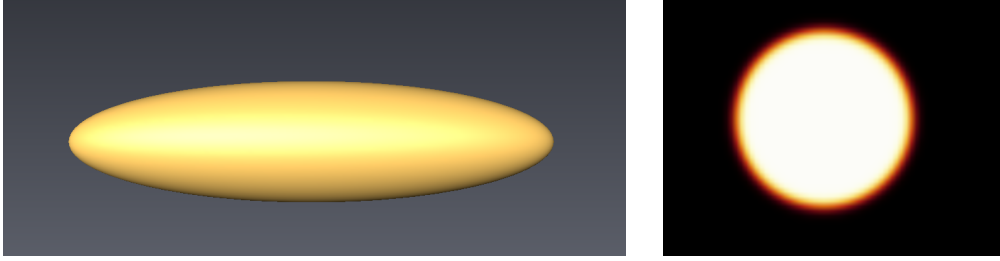


Figure 1: Left: Volume rendering of the anisotropic function  $\omega g_{r_0, r_1}$  corresponding to the action of the filter  $\phi$  on a tubular segment, as in Theorem 1. Right: Cross-section of  $\phi$ .

**Theorem 1.** Let  $\epsilon > 0$ ,  $\phi \in L^1(\mathbb{R}^3)$  be a radial function such that  $\xi \mapsto \|\xi\|^2 \hat{\phi}(\xi)$  is absolutely integrable and  $D^\alpha \phi \in L^1(\mathbb{R}^3)$  for all  $|\alpha| \leq 2$  and set

$$\omega(y, z) = \int_{\mathbb{R}} \phi(x, y, z) dx. \quad (7)$$

We have the following facts.

(i) If  $|(\mathbf{x} - \mathbf{x}_k) \cdot (R_k^T \mathbf{e}_1)| + r_0 < l$ , then

$$|(T_{\mathbf{x}_k} \mathcal{R} f_{l, L, r} * \phi)(\mathbf{x}) - g_r * \omega(y(\mathbf{x}_0), z(\mathbf{x}_0))| \leq \|g_r\|_1 \epsilon.$$

(ii) For every  $\mathbf{x}$  as in the previous item we have that

$$|(T_{\mathbf{x}_k} \mathcal{R} f_{l, L, r} * h)(\mathbf{x}) - g_r * \Delta_{y, z} \omega(y(\mathbf{x}_0), z(\mathbf{x}_0))| < 3 \|g_r\|_1 \epsilon$$

where,  $\Delta_{y, z} = \frac{\partial^2}{\partial y^2} + \frac{\partial^2}{\partial z^2}$ .

(iii) If  $0 < r_0 < r_1$ , where  $|(\mathbf{x} - \mathbf{x}_k) \cdot (R^T \mathbf{e}_1)| + r_1 < l$ , then

$$\left| (T_{\mathbf{x}_k} \mathcal{R} f_{l, L, r} * \phi)(\mathbf{x}) - \frac{1}{C} T_{\mathbf{x}_k} \mathcal{R} f_{l, L, r} * \mathcal{R}(\omega g_{r_0, r_1})(\mathbf{x}) \right| \leq \|g_r\|_1 \epsilon, \quad (8)$$

and

$$\left| (T_{\mathbf{x}_k} \mathcal{R} f_{l, L, r} * h)(\mathbf{x}) - \frac{1}{C} T_{\mathbf{x}_k} \mathcal{R} f_{l, L, r} * \mathcal{R}((\Delta_{y, z} \omega) g_{r_0, r_1})(\mathbf{x}) \right| < 3 \|g_r\|_1 \epsilon, \quad (9)$$

where  $C = \int_{\mathbb{R}} g_{r_0, r_1}(x) dx$ .

Before presenting the proof of Theorem 1, we will make some remarks to highlight the significance of the theorem.

Part (ii) of the theorem states that filtering the tubular segment using the 3D Isotropic Laplacian filter  $h$  is equivalent to applying the 2D Laplacian on the cross-section of the tubular structure  $T_{\mathbf{x}_i} \mathcal{R}f_{l,L,r}$ . Part (iii) states that filtering using the 3D isotropic filters  $\phi$  and  $h$  is equivalent to applying directional filters that automatically align themselves with the axis of the tubular structure (see Fig. 2.2). The orientation of the tubular segment is determined by the rotation  $R_k$  which orients its main axis along the direction  $R_k^T \mathbf{e}_1$ . According to (iii), the main axis of the directional filters  $\mathcal{R}_k(\omega g_{r_0,r_1})$  and  $\mathcal{R}_k((\Delta_{y,z}\omega)g_{r_0,r_1})$  is also parallel to  $R_k^T \mathbf{e}_1$ . This is why we claim that filtering with the radial filters  $\phi$  and  $h$  is equivalent to filtering with the directional filters  $\frac{1}{C} \mathcal{R}_k(\omega g_{r_0,r_1})$  and  $\frac{1}{C} \mathcal{R}_k((\Delta_{y,z}\omega)g_{r_0,r_1})$ , respectively, which are automatically aligned with the tubular structure locally at the point  $\mathbf{x}$ . The former of the two filters acts as a directional lowpass, bandpass or highpass filter depending on the frequency selectivity of  $\phi$ . The latter filter acts as a 2D Laplacian on a plane perpendicular to the direction of the tubular structure as (ii) shows.

Note that the outcome of the filtering process of the tubular segment using  $\phi$  and  $h$  depends only on the relative position of the point  $\mathbf{x}$  with respect to the cross-section of the tubular containing  $\mathbf{x}$  and on the properties of this cross-section. The similarity of the action of the filters  $\phi$  and  $h$  to truly directional filters is due solely to the geometry of the tubular segment, as one can verify by the proof of Theorem 1 below. Thus, our result establishes that a seemingly directionally insensitive system of atoms acts as a directional filter in certain conditions and is able to detect the geometric content associated with highly anisotropic objects. This ability to detect the geometry of elongated features is somewhat reminiscent of the properties of directional multiscale transform such the continuous shearlet transform, which was recently applied to detect the geometry of singularities of functions and distributions of several variables [9, 10]. However, there is an important difference here: the shearlet result for the detection of singularities is valid only asymptotically, when the scale variable tends to zero, whereas the result we derive here is valid over a range of scale associated with the spatial dimensions of the objects of interest.

In Section 3, we will briefly discuss the implications of these theoretical observations for the segmentation of tubular structures in biomedical images.

### 2.3. Proof of Theorem 1

We can now prove Theorem 1.

(i) Without loss of generality, we can take  $\mathbf{x}_0 = (0, y_{0,1}, z_{0,1})$ . A direct calculation gives that

$$f_{l,L,r} * \phi(\mathbf{x}_0) = \int_{\mathbb{R}} \int_{\mathbb{R}} g_r(y, z) \left( \int_{\mathbb{R}} g_{l,L}(x) \phi(-x, y_{0,1} - y, z_{0,1} - z) dx \right) dy dz.$$

Using (7) it follows that

$$\begin{aligned} & f_{l,L,r} * \phi(\mathbf{x}_0) - g_r * \omega(y_{0,1}, z_{0,1}) \\ &= \int_{\mathbb{R}^2} g_r(y, z) \left( \int_{\mathbb{R}} g_{l,L}(x) \phi(-x, y_{0,1} - y, z_{0,1} - z) dx - \omega(y_{0,1} - y, z_{0,1} - z) \right) dy dz. \end{aligned}$$

We can split the above integral by integrating over two complementary radial regions:

$$\int_{\mathbb{R}} g_{l,L}(x) \phi(-x, y_{0,1} - y, z_{0,1} - z) dx = \int_{|x| \leq r_0} (\dots) + \int_{|x| > r_0} (\dots).$$

Consequently, using the fact that  $g_{l,L}(x) = 1$  for all  $|x| \leq r_0$ , we have

$$\begin{aligned} & f_{l,L,r} * \phi(\mathbf{x}_0) - g_r * \omega(y_{0,1}, z_{0,1}) \\ &= \int_{\mathbb{R}} \int_{\mathbb{R}} g_r(y, z) \left[ \int_{|x| > r_0} [g_{l,L}(x) - 1] \phi(-x, y_{0,1} - y, z_{0,1} - z) dx \right] dy dz. \end{aligned}$$

Observing that  $0 \leq g_{l,L}(x) \leq 1$  for all  $x$  and  $\int_{|x| > r_0} |\phi| < \epsilon$  (Lemma 1), we conclude that

$$|f_{l,L,r} * \phi(\mathbf{x}_0) - g_r * \omega(y_{0,1}, z_{0,1})| \leq \|g_r\|_1 \epsilon.$$

This inequality combined with (5) proves part (i).

(ii) We begin by showing that the first term of the sum in the right-hand side of (6) is less than  $2\epsilon$ :

$$\begin{aligned} & \frac{\partial^2}{\partial x^2} (g_{l,L} g_r * \phi)(\mathbf{x}_0) \\ &= \left( g_r \frac{\partial^2 g_{l,L}}{\partial x^2} \right) * \phi(\mathbf{x}_0) \\ &= \int_{\mathbb{R}} \int_{\mathbb{R}} g_r(y, z) \left( \int_{\mathbb{R}} \frac{\partial^2 g_{l,L}}{\partial x^2}(x) \phi(-x, y_{0,1} - y, z_{0,1} - z) dx \right) dy dz \quad (10) \end{aligned}$$

and again we write

$$\int_{\mathbb{R}} \frac{\partial^2 g_{l,L}}{\partial x^2}(x) \phi(-x, y_{0,1} - y, z_{0,1} - z) dx = \int_{|x| \leq r_0} (\dots) + \int_{|x| > r_0} (\dots).$$

The first of the two terms in the integral above vanishes because  $g_{l,L}(x) = 1$  for all  $|x| < l$ . To estimate the second term we apply twice integration by parts using  $g_{l,L}(\pm L) = g'_{l,L}(\pm r_0) = g'_{l,L}(\pm L) = 0$  and  $g_{l,L}(\pm r_0) = 1$ :

$$\begin{aligned} & \int_{|x| > r_0} \frac{\partial^2 g_{l,L}}{\partial x^2}(x) \phi(-x, y_{0,1} - y, z_{0,1} - z) dx \\ &= \int_{|x| > r_0} \frac{\partial^2 \phi}{\partial x^2}(-x, y_{0,1} - y, z_{0,1} - z) g_{l,L}(x) dx + \frac{\partial \phi}{\partial x}(r_0, y_{0,1} - y, z_{0,1} - z). \end{aligned}$$

Thus we have that:

$$\left| \int_{|x| > r_0} \frac{\partial^2 g_{l,L}}{\partial x^2}(x) \phi(-x, y_{0,1} - y, z_{0,1} - z) dx \right| < 2\epsilon.$$

Using eqs. (6) and (10) we conclude that:

$$|(T_{\mathbf{x}_k} \mathcal{R}_k f_{l,L,r} * h)(\mathbf{x}) - \Delta_{y,z}(f_{l,L,r} * \phi)(\mathbf{x}_0)| < 2\|g_r\|_1 \epsilon. \quad (11)$$

Since  $D^\alpha \phi \in L^1(\mathbb{R}^3)$  for all  $|\alpha| \leq 2$ , we have that

$$\Delta_{y,z}(f_{l,L,r} * \phi)(\mathbf{x}_0) = f_{l,L,r} * (\Delta_{y,z}\phi)(\mathbf{x}_0) \quad (12)$$

and, hence,

$$\int_{\mathbb{R}} \Delta_{y,z}\phi(-x, y_{0,1} - y, z_{0,1} - z) dx = \Delta_{y,z}\omega(y_{0,1} - y, z_{0,1} - z),$$

for all  $y, z \in \mathbb{R}$ . It follows that

$$\begin{aligned} & \int_{\mathbb{R}} \Delta_{y,z}\phi(-x, y_{0,1} - y, z_{0,1} - z) g_{l,L}(x) dx - \Delta_{y,z}\omega(y_{0,1} - y, z_{0,1} - z) \\ &= \int_{|x| > r_0} [g_{l,L}(x) - 1] \Delta_{y,z}\phi(-x, y_{0,1} - y, z_{0,1} - z) dx. \end{aligned}$$

Now, arguing as in the proof of part (i) and using eq. (12), we obtain that

$$|f_{l,L,r} * (\Delta_{y,z}\phi)(\mathbf{x}_0) - g_r * (\Delta_{y,z}\omega)(y_{0,1}, z_{0,1})| \leq \|g_r\|_1 \epsilon.$$

Combining the previous inequality with (11), we complete the proof of part (ii).

(iii) Using again the change of variables leading to eq. (4) we have that

$$T_{\mathbf{x}_k} \mathcal{R}_k f_{l,L,r} * \mathcal{R}_k (\omega g_{r_0,r_1})(\mathbf{x}) = f_{l,L,r} * (\omega g_{r_0,r_1})(\mathbf{x}_0).$$

Now, let  $x(\mathbf{x}_0)$  be the  $x$ -coordinate of  $\mathbf{x}_0$ . Then:

$$\begin{aligned} f_{l,L,r} * (\omega g_{r_0,r_1})(\mathbf{x}_0) &= g_r * \omega(y_{0,1}, z_{0,1}) \int_{\mathbb{R}} g_{l,L}(x(\mathbf{x}_0) - x) g_{r_0,r_1}(x) dx \\ &= C g_r * \omega(y_{0,1}, z_{0,1}), \end{aligned} \quad (13)$$

since  $g_{l,L}(x(\mathbf{x}_0) - x) = 1$  for all  $|x| < r_1$ , due to the observations that  $|(\mathbf{x} - \mathbf{x}_k) \cdot (R_k^T \mathbf{e}_1)| + r_1 < l$ . Combining eq. (13) and part (i) we derive eq. (8). Eq. (9) can be derived with similar arguments. This completes the proof of Theorem 1.  $\square$

#### 2.4. Other results

The following observation is useful to determine the filter  $h$  so that it can accurately capture the change in the sign of  $\Delta_{y,z} g_r$ . Here we provide a formal statement on the dependence of the choice of  $r_0$  on  $r$ . Recall, that the latter is a metric indicative of the thickness of the tubular structure. Failure to choose the filter  $\phi$  with the appropriate bandwidth  $r_0$  will result in aliasing errors that will compromise the detection of the surface of the tubular structure.

**Proposition 1.** *Assume that the hypotheses of Theorem 1 hold true and suppose that  $|1 - \hat{\phi}(\xi)| < \epsilon$  for a.e.  $\|\xi\| < \rho$ , where  $\rho$  is determined by*

$$\int_{\|(\xi_2, \xi_3)\| > \rho} \hat{g}_r(\xi_2, \xi_3) (\xi_2^2 + \xi_3^2) d\xi_2 d\xi_3 < \frac{\epsilon}{1 + \|\phi\|_1}. \quad (14)$$

Then, for every  $x_i$  and rotation  $R_k$ , we have that

$$|(T_{\mathbf{x}_i} \mathcal{R}_k f_{l,L,r} * h)(\mathbf{x}) - \Delta_{y,z} g_r(y(\mathbf{x}_0), z(\mathbf{x}_0))| \leq (3\|g_r\|_1 + 1)\epsilon$$

for every  $\mathbf{x}$  that is sufficiently far from the endpoints of the tubular structure  $T_{\mathbf{x}_i} \mathcal{R}_k f_{l,L,r}$ , in the sense that  $|(\mathbf{x} - \mathbf{x}_i) \cdot (R_k^T \mathbf{e}_1)| + r_0 < l$ .

*Proof:* A direct computation shows that

$$\begin{aligned}
& |(T_{\mathbf{x}_i} \mathcal{R}_k f_{l,L,r} * h)(\mathbf{x}) - \Delta_{y,z} g_r(y(\mathbf{x}_0), z(\mathbf{x}_0))| \\
&= |(T_{\mathbf{x}_i} \mathcal{R}_k f_{l,L,r} * h)(\mathbf{x}) - g_r * \Delta_{y,z} \omega(y(\mathbf{x}_0), z(\mathbf{x}_0)) \\
&\quad - \Delta_{y,z} g_r(y(\mathbf{x}_0), z(\mathbf{x}_0)) + g_r * \Delta_{y,z} \omega(y(\mathbf{x}_0), z(\mathbf{x}_0))| \\
&\leq |(T_{\mathbf{x}_i} \mathcal{R}_k f_{l,L,r} * h)(\mathbf{x}) - g_r * \Delta_{y,z} \omega(y(\mathbf{x}_0), z(\mathbf{x}_0))| \\
&\quad + |g_r * \Delta_{y,z} \omega(y(\mathbf{x}_0), z(\mathbf{x}_0)) - \Delta_{y,z} g_r(y(\mathbf{x}_0), z(\mathbf{x}_0))|.
\end{aligned}$$

By part (ii) of Theorem 1 we know that the first term of the sum above does not exceed  $3\|g_r\|_1 \epsilon$ . Next, we will show that the second term in the sum is bounded above by  $3\epsilon$ . By computing the Fourier transform of second term, we get

$$(g_r * \Delta_{y,z} \omega - \Delta_{y,z} g_r)^\wedge(\xi_2, \xi_3) = \widehat{g}_r(\xi_2, \xi_3)(\xi_2^2 + \xi_3^2) \widehat{\omega}(\xi_2, \xi_3) - \widehat{g}_r(\xi_2, \xi_3)(\xi_2^2 + \xi_3^2). \quad (15)$$

We have that:

$$\begin{aligned}
& \int_{\mathbb{R}^2} |\widehat{g}_r(\xi_2, \xi_3)(\xi_2^2 + \xi_3^2) \widehat{\omega}(\xi_2, \xi_3) - \widehat{g}_r(\xi_2, \xi_3)(\xi_2^2 + \xi_3^2)| d\xi_2 d\xi_3 \\
&= \int_{\mathbb{R}^2} \widehat{g}_r(\xi_2, \xi_3)(\xi_2^2 + \xi_3^2) |\widehat{\omega}(\xi_2, \xi_3) - 1| d\xi_2 d\xi_3 \\
&\leq \int_{\|(\xi_2, \xi_3)\| \leq \rho} \widehat{g}_r(\xi_2, \xi_3)(\xi_2^2 + \xi_3^2) |\widehat{\omega}(\xi_2, \xi_3) - 1| d\xi_2 d\xi_3 \\
&\quad + \int_{\|(\xi_2, \xi_3)\| \geq \rho} \widehat{g}_r(\xi_2, \xi_3)(\xi_2^2 + \xi_3^2) (|\widehat{\omega}(\xi_2, \xi_3)| + 1) d\xi_2 d\xi_3.
\end{aligned}$$

Now, using the assumption that  $|1 - \widehat{\phi}(\xi)| < \epsilon$  for a.e.  $\|\xi\| < \rho$ , (14), (15) and the fact  $\widehat{\omega}(\xi_2, \xi_3) = \widehat{\phi}(0, \xi_2, \xi_3)$  for a.e.  $(\xi_2, \xi_3)$ , we conclude that

$$|(T_{\mathbf{x}_i} \mathcal{R}_k f_{l,L,r} * h)(\mathbf{x}) - \Delta_{y,z} g_r(y(\mathbf{x}_0), z(\mathbf{x}_0))| \leq (3\|g_r\|_1 + 1)\epsilon \quad (16)$$

This completes the proof of Proposition 1.  $\square$

An example of a filter  $\phi$  satisfying the assumptions of Proposition 1 is given by

$$\widehat{\phi}(\xi) = P_n(C_{n,\sigma} \|\xi\|^2) e^{-C_{n,\sigma} \|\xi\|^2},$$

where  $P_n$  is the Taylor polynomial of degree  $n$  associated with the exponential function  $e^x$ , the constant  $C_{n,\sigma}$  is

$$C_{n,\sigma} = \frac{2n+1}{2(K\sigma)^2},$$

and  $\sigma$  is a parameter associated with a notion of scale. This filter belongs to the class of Hermite Distributed Approximating Functions that were originally proposed by Hoffman *et. al.* in [13]. The choice of the constant  $C_{n,\sigma}$  places the inflection point of the radial profile of  $\hat{\phi}$  firmly at radius  $K\sigma$  from the origin, regardless of the value of  $n$ . As  $n$  increases to  $\infty$  (cf. [1, Remark 3.4]), the width of the radial profile of the transition band of  $\hat{\phi}$  is proportional to  $\frac{1}{n}$ . This transition band also contains the inflection point of the radial profile of  $\hat{\phi}$ , for every  $n$ . Moreover, as  $n$  grows, the values of  $\hat{\phi}$  tend to 1 at every point in the ball centered at the origin with radius  $K\sigma$  ([1, Th. 3.7]). In a nutshell,  $\hat{\phi}$  asymptotically behaves like an isotropic ideal low pass filter.

So far our analysis was focused on a single segment  $T_{\mathbf{x}_i}\mathcal{R}_k f_{l,L,r}$  of the tubular structure  $I$  given by (2). The proposed filters  $\phi$  and  $h$  can be applied to the entire tubular structure  $I$ . Recall that, in Theorem 1, we assumed that the point  $\mathbf{x}$  is close only to a single tubular segment of  $I$ . Due to the spatial localization of the filters  $\phi$  and  $h$ , each tubular segment can be processed independently of the others. This observation leads to the following corollary.

**Corollary 1.** *Under the assumptions of Theorem 1, we have that*

$$|(I * \phi)(\mathbf{x}) - g_r * \omega(y(\mathbf{x}_0), z(\mathbf{x}_0))| = O(\epsilon),$$

and

$$|(I * h)(\mathbf{x}) - g_r * \Delta_{y,z}\omega(y(\mathbf{x}_0), z(\mathbf{x}_0))| = O(\epsilon),$$

where  $\mathbf{x}_0 = R_k(\mathbf{x} - \mathbf{x}_i)$  and where the index  $i$ , the cross-section  $g_r$  and the rotation  $R_k$  correspond to the most proximal segment  $T_{\mathbf{x}_i}\mathcal{R}_k f_{l,L,r}$  of  $I$  to  $\mathbf{x}$ . Consequently, we have that

$$|(I * h)(\mathbf{x}) - \Delta_{y,z}g_r(y(\mathbf{x}_0), z(\mathbf{x}_0))| = O(\epsilon).$$

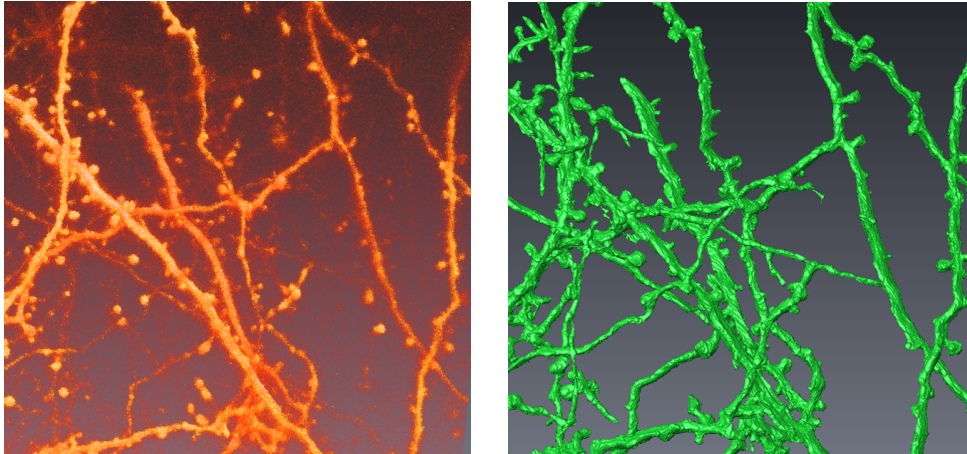


Figure 2: Left: Dendritic branches from a neuronal tissue acquired using multi-photon fluorescent microscopy showing spines (courtesy of Professor Tara Keck, King’s College, London, UK). The tiny round protrusions located at the dendritic branches are called spines and play a critical role in learning and memory models. Right: Segmentation obtained using the method in [12] which selects the training regions for the classification algorithm based on the last assertion of Corollary 1.

### 3. Applications to image segmentation

The ideas presented above provide the theoretical justification for the development of algorithms of segmentation of vessel-like structures developed by the authors and their collaborators [15, 14]. In particular, the isotropic Laplacian filters we presented in Sec. 2 are an essential part in a segmentation algorithm which was implemented with a Support Vector Machine (SVM) to process 3D images from the Diadem dataset. The Diadem dataset is used as a benchmark in the computational neuroscience community to test segmentation and centerline tracing algorithm on complex dendritic arbors from images of various areas of the brain [2].

To describe the role of such 3D-isotropic filters for the detection of tubular structure in these applications, we assume that cross-sectional intensity profile functions  $g_r$  have an “inflection point” at which the sign of  $\Delta_{y,z}g_r$  changes from negative to positive. Here we stress that widely accepted models of intensity profiles of tubular structures do not identify a “skin”, that is, a discontinuous boundary of the tubular structure separating the inside from the outside. Instead, the image intensity values in the tubular structure gradually drop from a peak value at the centerline of the structure down to

the range of background values. This principle is reflected in the adopted model of cross-sectional intensity values in and out of the tubular structure, formally presented by  $g_r$  in Sec. 2. Hence, we *postulate that the ‘boundary’ of the tubular structure is located at some intermediate radial distance from the centerline of the structure*, preferably at the radial distance of this “inflection surface” from the centerline. Then, based on the theoretical predictions of Corollary 1, we expect  $I * h$  to have positive sign right outside the boundary of the tubular structure, because  $I * h$  is practically equal to  $\Delta_{y,z}g_r$ , the 2D-Laplacian on the cross-section of  $I$  containing  $\mathbf{x}$ . Further away from this boundary, the error of the approximation of the values of  $\Delta_{y,z}g_r$  predicted by Proposition 1 and the response of the application of  $h$  to its other proximal segments force the sign of  $I * h$  to vary. According to these remarks, the problem of segmenting a tubular structure from the background is not posed as an edge detection problem in 3D. Rather, the successful extraction of the geometric features of the tubular structures can be achieved using a set of Laplacian isotropic filters with varying bandwidths, as Proposition 1 suggests.

The justification of the adopted model of tubular structure is verified indirectly by the high accuracy of our segmentations and centerline tracing reported in [15, 14, 11, 12] where the performance of this approach is compared with state-of-the-art methods from the literature. For example, the application of our centerline tracing algorithm in [14] to volumes from the Diadem set yields Miss-Extra-Score (MES) = 0.93 as compared with the state-of-the-art algorithm of Xie et al. [26] that yields MES = 0.86 (MES is a standard performance metric, where higher values indicate better performance, cf. [14]). One of the advantages of our theoretical formalization is to enable the automatization of the selection process for the training subsets of the SVM-classifier used in the segmentation algorithm. We illustrate an example of application of this algorithm in Fig. 2, showing the segmentation of a complex dendritic network from a brain tissue acquired using two-photon fluorescent microscopy. These images are acquired *in vivo* and are very challenging to segment due to the high level of noise produced during data acquisition. Note that the flexibility permitted by our modelling of tubular structures in Sec. 2 enables us to derive an algorithmic approach which is effective not only for the detection of the main dendritic branches, but also for the detection of their fine-scale details. As the figure shows, the segmentation algorithm is able to capture also the *dendritic spines*, tiny protrusions emerging from dendritic branches which play a very significant

role in many cognitive and pharmacological models of the brain.

**Acknowledgment:** This work was supported in part by NSF-DMS 1320910, 0915242, 1008900, 1005799 and by NHARP-003652-0136-2009. We thank Prof. T. Keck of King’s College, London, UK, for providing the data of Fig. 2 and P. Hernandez-Herrera for sharing his segmentation algorithm from [12]. We also thank Prof. I.A. Kakadiaris of the University of Houston and Prof. F. Laezza of the University of Texas Medical Branch in Galveston for helpful discussions on neuroscience imaging.

## References

- [1] Bodmann, B., Hoffman, D., Kouri, D., Papadakis, M., 2007. Hermite distributed approximating functionals as almost-ideal low-pass filters. *Sampling Theory in Image and Signal Processing* 7, 15–38.
- [2] Brown, K., Barrionuevo, G., Canty, A., Paola, V., Hirsch, J., Jefferis, G., Lu, J., Snippe, M., Sugihara, I., Ascoli, G., 2011. The DIADEM data sets: representative light microscopy images of neuronal morphology to advance automation of digital reconstructions. *Neuroinformatics* 9 (2-3), 143–157.
- [3] Candès, E., Donoho, David L., 1999. Ridgelets: a key to higher-dimensional intermittency? *Philosophical Transactions of the Royal Society A: Mathematical, Physical and Engineering Sciences* 357 (1760), 2495–2509.
- [4] Candès, E. J., Donoho, D. L., 2004. New tight frames of curvelets and optimal representations of objects with piecewise  $C^2$  singularities. *Comm. Pure Appl. Math.* 57 (2), 219–266.
- [5] Candès, E. J., Donoho, D. L., 2005. Continuous curvelet transform: I. resolution of the wavefront set. *Appl. Comp. Harm. Analysis* 19, 162–197.
- [6] Donoho, D., Huo, X., 2002. Beamlets and multiscale image analysis. In: Barth, T. J., Chan, T., Haimes, R. (Eds.), *Multiscale and Multiresolution Methods*. Vol. 20 of *Lecture Notes in Computational Science and Engineering*. Springer Berlin Heidelberg, pp. 149–196.

- [7] Farah, M., 2000. The cognitive neuroscience of vision. Blackwell Publishers, Malden, MA.
- [8] Guo, K., Labate, D., 2007. Optimally sparse multidimensional representation using shearlets. *SIAM J. Math. Analysis* 39 (1), 298–318.
- [9] Guo, K., Labate, D., 2009. Characterization and analysis of edges using the continuous shearlet transform. *SIAM J. Imaging Sciences* 2 (3), 959–986.
- [10] Guo, K., Labate, D., 2012. Characterization of piecewise smooth surfaces using the 3D continuous shearlet transform. *J. Fourier Anal. Appl.* 18, 488–516.
- [11] Hernandez-Herrera, P., Papadakis, M., Kakadiaris, I., 2014. Multi-scale segmentation of neurons based on one-class classification, under review.
- [12] Hernandez-Herrera, P., Papadakis, M., Kakadiaris, I., Apr 28 - May 2 2014. Segmentation of neurons based on one-class classification. In: *Proc. IEEE International Symposium in Biomedical Imaging*. Beijing, China.
- [13] Hoffman, D. K., Nayar, N., Sharafeddin, O. A., Kouri, D. J., 1991. Analytic banded approximation for the discretized free propagator. *J. Phys. Chem.* 95, 8299–8305.
- [14] Jimenez, D., Labate, D., Kakadiaris, I., Papadakis, M., 2014. Improved automatic centerline tracing for dendritic and axonal structures, *Neuroinformatics*. in press.
- [15] Jimenez, D., Papadakis, M., Labate, D., Kakadiaris, I., April 8-11 2013. Improved automatic centerline tracing for dendritic structures. In: *Proc. International Symposium on Biomedical Imaging: From Nano to Macro*. San Francisco, CA, pp. 1050–1053.
- [16] Koller, T., Gerig, G., Szekely, G., Dettwiler, D., Jun 1995. Multiscale detection of curvilinear structures in 2-d and 3-d image data. In: *Computer Vision, 1995. Proceedings., Fifth International Conference on Computer Vision*. pp. 864–869.

- [17] Krissian, K., Malandain, G., Ayache, N., Vaillant, R., Troussset, Y., 2000. Model based detection of tubular structures in 3d images. *Computer Vision and Image Understanding* 80 (2), 130–171.
- [18] Kutyniok, G., Labate, D., 2009. Resolution of the wavefront set using continuous shearlets. *Trans. Amer. Math. Soc.* 361, 2719–2754.
- [19] Kutyniok, G., Lim, W.-Q., 2011. Compactly supported shearlets are optimally sparse. *Journal of Approximation Theory* 163 (11), 1564–1589.
- [20] Labate, D., Laezza, F., Ozcan, B., Negi, P., Papadakis, M., 2014. Efficient processing of fluorescence images using directional multiscale representations. *Math. Model. Nat. Phenom.* 9 (5), 177–193.
- [21] Labate, D., Lim, W., Kutyniok, G., Weiss, G., January 2005. Sparse multidimensional representation using shearlets. In: Unser, M. (Ed.), *Proc. Wavelets XI*. Vol. 5914 of *SPIE Proceedings*. pp. 247–255.
- [22] Marr, D., 1982. *Vision, A computational investigation into the human representation and processing of visual information*. W.H. Freeman and Co., New York, NY.
- [23] Ozcan, B., Jiménez, D., Hernandez-Herrera, P., Labate, D., Kakadiaris, I., Papadakis, M., September 2013. Directional and non-directional sparse representations for the characterization of morphological properties of neurons in fluorescent microscopy images. In: *Proc. SPIE Proceedings, Wavelets and Sparsity XV*. Vol. 8858. San Diego.
- [24] Sündermann, F., Lotter, S., Lim, W.-Q., Golovyashkina, N., Brandt, R., Kutyniok, G., 2014. Shearlet analysis of confocal laser-scanning microscopy images to extract morphological features of neurons. In: Bakota, L., Brandt, R. (Eds.), *Laser Scanning Microscopy and Quantitative Image Analysis of Neuronal Tissue*. Vol. 87 of *Neuromethods*. Springer New York, pp. 293–303.
- [25] Wandell, B., 1995. *Foundations of vision*. Sinauer Associates, Inc., Sunderland, Massachusetts.
- [26] Xie, X., Zheng, W.-S., Lai, J., Yuen, P., Suen, C., July 2011. Normalization of face illumination based on large-and small-scale features. *IEEE Transactions on Image Processing* 20 (7), 1807–1821.